

High resolution near-IR spectroscopy of FGK stars

Daniel Thaagaard Andreasen

March 9, 2017

*To Linnea, Henriette, and Rico
For always supporting me*

CONTENTS

Contents	iii
Abstracts	v
List of Figures	vi
List of Tables	vi
1 Introduction	1
1.1 Planet host stars	3
1.2 Atmospheric parameters	3
2 Theory	5
2.1 Stellar structure	5
2.2 Stellar atmosphere	7
2.2.1 The equivalent width	7
2.2.1.1 Temperature dependence	7
2.2.1.2 Pressure dependence	8
2.2.1.3 Abundance dependence	10
2.2.1.4 Microturbulence	11
2.2.2 Stellar parameters for FGK stars	12
2.2.2.1 Line list and atomic data	12
2.2.2.2 Measuring EW	12
2.2.2.3 Determining abundances with MOOG	12
Bibliography	13

ABSTRACTS

LIST OF FIGURES

2.1	An absorption line centered at λ_0 normalized at the flux level F_c . The area of the absorption line to the left is equal to the blue shaded area in the rectangle to the right with width EW.	8
2.2	The EW for a Fe I and Fe II line with increasing T_{eff} . The two lines have similar EW in the Sun and are found in the optical part of the spectrum.	9
2.3	<i>Upper panel:</i> Curve of growth for same Fe II used in Figure 2.2 on page 9 for four different $\log g$ values. Here it is the weak lines mostly affected by the change in $\log g$. <i>Lower left panel:</i> Synthetic spectra of the same line. The colour scale is the same. <i>Lower right:</i> The abundance for the line at different $\log g$. A strong correlation (0.40) is seen.	10
2.4	<i>Upper panel:</i> Curve of growth of the same Fe I line as used in Figure 2.2 on page 9. Four points are marked which is shown in the <i>lower panel</i> as a synthetic spectral line. The RW (proxy for EW) is clearly increasing with $\log gf$ (proxy for abundance).	11
2.5	Curve of growth for three different values of ξ_{micro} . The EW is increasing with increasing ξ_{micro}	12

LIST OF TABLES

INTRODUCTION

Effective temperature (T_{eff}), surface gravity ($\log g$), and metallicity ($[M/H]$, where iron is normally used as a proxy) are fundamental atmospheric parameters necessary to characterise a single star, and to determine other indirectly fundamental parameters such as mass, radius, and age from stellar evolution models (see e.g. [Baraffe et al., 2015](#); [Dotter et al., 2008](#); [Girardi et al., 2000](#)). Precise and accurate stellar parameters are also essential in exoplanet searches. Planetary radius and mass are mainly found from transit lightcurve analysis and radial velocity analysis, respectively. The determination of the mass of the planet implies a knowledge of the stellar mass, while the measurement of the radius of the planet is dependent on our capability to derive the radius of the star (see e.g. [Ammler-von Eiff et al., 2009](#); [Torres et al., 2012, 2008](#)).

The derivation of precise stellar atmospheric parameters is not a simple task. Different approaches often lead to discrepant results (see e.g. [Lebzelter et al., 2012](#); [Santos et al., 2013](#); [Torres et al., 2010](#)). Interferometry is usually considered an accurate method for deriving stellar radii (see e.g. [Boyajian et al., 2012](#)); however, it is only applicable for bright nearby stars. Asteroseismology, on the other hand, reveals the inner stellar structure by observing the stellar pulsations at the surface. From asteroseismology it is possible to measure the surface gravity and mean density, and therefore to calculate mass and radius with high precision (see e.g. [Kjeldsen and Bedding, 1995](#)). However, for stars on the main sequence asteroseismic methods can typically only be applied to FG stars, since the oscillation modes of K and M dwarfs are likely too weak to be detected even with high precision spectroscopy or photometry. Moreover, the effective temperature is needed when applying asteroseismology in order to obtain the surface gravity and the mean density.

A crucial parameter for the indirect determination of stellar bulk properties is the T_{eff} . In that respect, the infrared flux method (IRFM) has proven to be reliable for FGK dwarf and subgiant stars. For higher accuracy the IRFM needs a priori knowledge of the bolometric flux, reddening, surface gravity, and stellar metallicity (Blackwell and Shallis, 1977; Casagrande et al., 2010; Ramírez and Meléndez, 2005).

Finally, the use of high resolution spectroscopy along with stellar atmospheric models is an extensively tested method that allows the derivation of the fundamental parameters of a star (see e.g. Santos et al., 2013; Valenti and Fischer, 2005). The procedure depends on the quality of the spectra, their resolution, and wavelength region. A fit to the overall spectrum can be applied for all spectral resolutions, but are often time consuming (see e.g. Recio-Blanco et al., 2006; Tsantaki et al., 2014). For resolutions higher than $\lambda/\Delta\lambda \sim 20\,000$ we can apply the equivalent width (EW) method (see e.g. Andreasen et al., 2017; Tsantaki et al., 2013, for details). However, while the latter approach is often faster than the synthetic fitting, it requires higher quality spectra, and the star to be slow rotating (below 10 km/s to 15 km/s).

Standard procedures are often used to derive stellar atmospheric parameters from high quality spectra in the optical (see e.g. Sousa et al., 2008; Valenti and Fischer, 2005). With the advancement of high resolution near-infrared (NIR) instruments, we will now be able to use a similar technique to that used in the optical part of the spectrum (see e.g. Bensby et al., 2014; Meléndez and Barbuy, 1999; Mucciarelli et al., 2013; Sousa et al., 2008; Tsantaki et al., 2013). At the moment, the GIANO spectrograph installed at *Telescopio Nazionale Galileo* (TNG) is already available (Origlia et al., 2014), as is the *infrared Doppler instrument* (IRD) installed at the Subaru telescope (Kotani et al., 2014), *Calar Alto high-Resolution search for M dwarfs with Exoearths with Near-infrared and optical Échelle Spectrographs* (CARMENES) for the 3.5 m telescope at Calar Alto Observatory (Quirrenbach et al., 2014), and *iShell* at the *InfraRed Telescope Facility* (Rayner et al., 2012, 2016). Three new spectrographs are planned for the near future: 1) The *CRyogenic InfraRed Echelle Spectrograph Upgrade Project* (CRIRES+) at the *Very Large Telescope* (VLT) (Follert et al., 2014) with expected first light in 2017, 2) *un SpectroPolarimètre Infra-Rouge A Near-InfraRed Spectropolarimeter* (SPIRou) at *The Canada-France-Hawaii Telescope* (CFHT) (Artigau et al., 2014; Delfosse et al., 2013) with expected first light in 2017 as well, and 3) *Near Infrared Planet Searcher* NIRPS at the ESO 3.6 m telescope in La Silla (Conod et al., 2016). The spectral resolutions for these spectrographs range between 50 000 and 100 000.

With the advance of the next generation NIR spectrographs, we are still preparing the data analysis of stellar spectra, in particular how to get reliable atmospheric parameters (see e.g. Andreasen et al., 2016; Lindgren et al., 2016; Önehag et al., 2012). The analysis of stellar spectra is well understood for FGK stars in the optical part of the spectrum, however some work still needs to be

done for the NIR part.

We continue our series of studies to explore the use of the NIR domain to derive stellar parameters for FGK and M stars. In particular, here we analyse the atlas of Arcturus and the spectrum of 10 Leo. For the analysis we use the iron line list presented in [Andreasen et al. \(2016\)](#) (referred to as Paper I). In Paper I we successfully tested our method on a slightly hotter star than the Sun, while in this work we aim to test the method on cooler stars. The strength of the NIR domain over the optical becomes clear when we move towards the cooler stars. Here we see less continuum depression and line blending due to in particular molecular features. Moreover, the cooler stars emit more light in the NIR domain than the optical, and with the lightest stars being intrinsically faint, we thus obtain the majority of the flux here.

1.1 Planet host stars

With the present diversity of exoplanets it becomes increasingly important to get an accurate and precise characterization of the planets in order to study them in samples and on an individual level. An accurate and precise characterization can give us an idea whether the planet is rocky, composed of water or gaseous.

1.2 Atmospheric parameters

THEORY

To encompass all theory regarding stellar structure, evolution, and their atmosphere is far beyond the scope of this thesis. Rather the theory needed is presented below with highlights on the most important aspects.

2.1 Stellar structure

The structure of a non-rotating spherical stars can be described by five rather simple differential equations (see e.g. [Kippenhahn and Weigert, 1994](#)) presented below:

1. Equation of Continuity

Relation between the mass, m , the density, ρ , at a symmetric shell at radius r

$$\frac{\partial r}{\partial m} = \frac{1}{4\pi r^2 \rho}. \quad (2.1)$$

2. Equation of Hydrostatic Equilibrium

The equation of hydrostatic equilibrium shows how a star in equilibrium is balanced between two forces. The inward force from gravity and the outward force from pressure, P ,

$$\frac{\partial P}{\partial m} = -\frac{Gm}{4\pi r^4}. \quad (2.2)$$

When working with asteroseismology a time dependent perturbation to this equation is added (see e.g. [Aerts et al., 2010](#), for a thorough discussion). However, this term is neglected here.

3. Equation of Energy Conservation

The equation of energy conservation shows how the energy is produced and lost throughout the star.

$$\boxed{\frac{\partial l}{\partial m} = \varepsilon - \varepsilon_\nu + \varepsilon_g} \quad (2.3)$$

where ε is the energy production in the center of the star, ε_ν is the energy lost by neutrinos which is always positive, ε_g is a source function of time-dependent terms, and l is the luminosity at m . ε_g comes from the fact that non-stationary shells can change its internal energy, and thus exchange mechanical energy with neighboring shells.

4. Equation of Energy Transport

Energy transportation throughout the star is described with the following equation

$$\boxed{\frac{\partial T}{\partial m} = -\frac{GmT}{4\pi r^4 P} \nabla_{\text{rad}}}, \quad (2.4)$$

where ∇_{rad} is the radiative temperature gradient, and T is the temperature. The value of the temperature gradient compared to the radiative temperature gradient tells if the energy is transported by convection or radiation. In our Sun the outer layer are convective while the inner layer are radiative.

5. Equation of Chemical Composition

In this last equation we see the evolution of an element, X_i , when it reacts with other elements with reaction rates r_{ji} and r_{ik}

$$\boxed{\frac{\partial X_i}{\partial t} = \frac{m_i}{\rho} \left(\sum_j r_{ji} - \sum_k r_{ik} \right)}. \quad (2.5)$$

Note that this is the only time-dependent equation of the five presented.

These five fundamental equations are implemented in stellar evolutionary codes, which we will use in later chapters. The many different codes that exist

take other things into account, e.g the star can rotate, and it may not always be in hydrostatic equilibrium (this is important if we want our star to pulsate). For simplicity we have only presented time-dependence in the Equation of Chemical Composition since timescales of rotation, pulsations, and activity are much shorter than the long timescale found in chemical composition changes.

2.2 Stellar atmosphere

Much of this Section is inspired by [Gray \(2005\)](#). While all the figures here were made by the author of this thesis, many of them can be found in [Gray \(2005\)](#) as well.

Write here about the formation of spectral lines...

2.2.1 The equivalent width

Measuring the equivalent width (EW) of spectral lines are important for some analysis of stellar spectra. The EW is a measure of the strength of the line, and dependent on the atmospheric conditions in where the spectral line is formed, such as T_{eff} , $\log g$, $[\text{Fe} / \text{H}]$, and ξ_{micro} .

The EW is mathematically described as integrating over the entire line, and assign this area to a rectangle from 0 to the continuum flux (F_c) with the width, EW. This is illustrated in Figure 2.1 on the following page and the equation below:

$$EW = \int_0^\infty \frac{F_c - F(\lambda)}{F_c} d\lambda, \quad (2.6)$$

where λ is the wavelength. This integral is assuming there is only one single line, hence the integral is over all wavelength. In practice the integral is calculated in small windows around a spectral line. See Section 2.2.2.2 on page 12 for more details on how this is performed in practice. The unit of the EW is the same as the wavelength used. Throughout this thesis we will use Ångström ($1\text{\AA} = 0.1\text{ nm}$) for the wavelength, and mÅ for the EW.

2.2.1.1 Temperature dependence

As mentioned above the EW depends on the atmospheric parameters. The dependence on T_{eff} is the strongest dependence. At low T_{eff} neutral elements, say Fe I, are the strongest lines as the number of ionized atoms are too small to contribute significantly to the EW. As T_{eff} increases Fe I is converted into ionized Fe II. Slowly, as the number of Fe I decreases so does the EW, and likewise as the number of Fe II increases so does the EW. This goes on until second ionized atoms, Fe III, are formed and the same situation arise again. This is illustrated in Figure 2.2 on page 9 where the EW of two iron lines, one

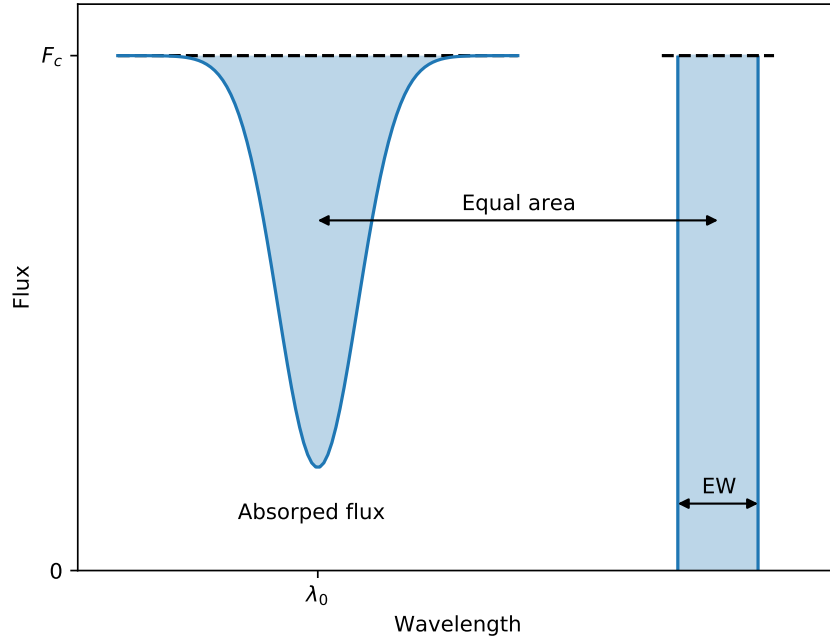


Figure 2.1: An absorption line centered at λ_0 normalized at the flux level F_c . The area of the absorption line to the left is equal to the blue shaded area in the rectangle to the right with width EW .

neutral and one ionized, are plotted against T_{eff} . These two lines have similar EW in the Sun: 46.2 mÅ and 53.9 mÅ for the Fe I and Fe II line respectively.

2.2.1.2 Pressure dependence

Pressure dependence in the stellar atmosphere can be related to the gravity dependence. There are many ways to measure the pressure, and thus the gravity which is what is ultimately the goal with the measurement of $\log g$. Below are listed some of the most common methods to measure $\log g$ from spectroscopy.

- Continuum: The Balmer jump is the only continuum feature sensitive enough to estimate the $\log g$.
- Hydrogen lines: Hydrogen profiles are pressure sensitive and can therefore be used to estimate $\log g$. However, the gravity dependence rapidly diminishes for temperatures above 10 000 K.

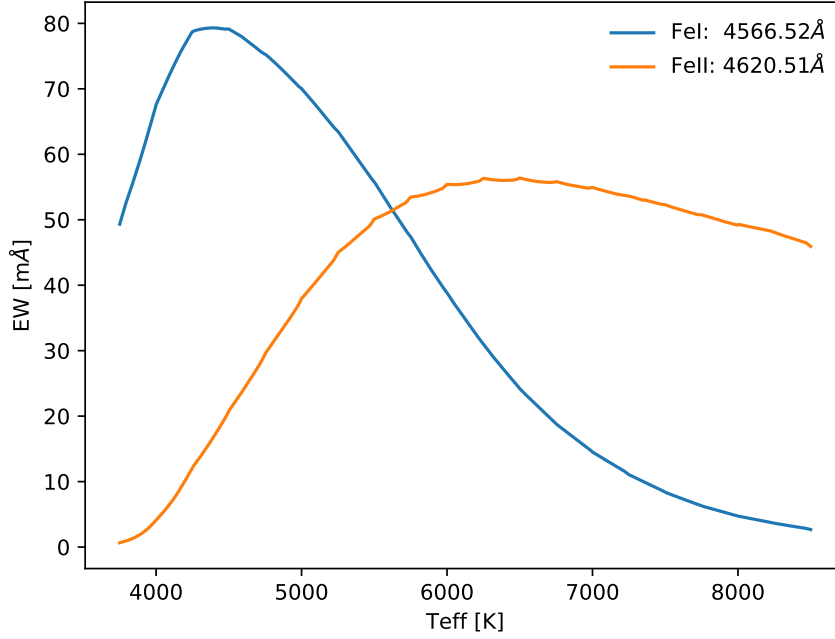


Figure 2.2: The EW for a Fe I and Fe II line with increasing T_{eff} . The two lines have similar EW in the Sun and are found in the optical part of the spectrum.

- Other strong lines: There exists other strong lines with pressure-broadened wings such as the Ca II H and K lines. These are better for cooler stars than the hydrogen lines described above.
- Weak lines: By comparing two stages of ionization for the same element it is possible to obtain $\log g$ using weaker or modestly strong lines.

In this thesis weak lines are used to measure $\log g$. More specifically a comparison between Fe I and Fe II lines are used. For FGK stars, as the atmosphere contracts (i.e. $\log g$ increases) the pressure likewise increases, which in turn means that both the gas pressure, P_g , and electron pressure, P_e , increases. Since hydrogen is the main electron contributor, but not fully ionized for these stars, the electron pressure is much smaller than the gas pressure. The gas pressure follows a simple empirical approximation with gravity:

$$P_g \simeq \text{constant } g^{2/3}, \quad (2.7)$$

where g is the gravity.

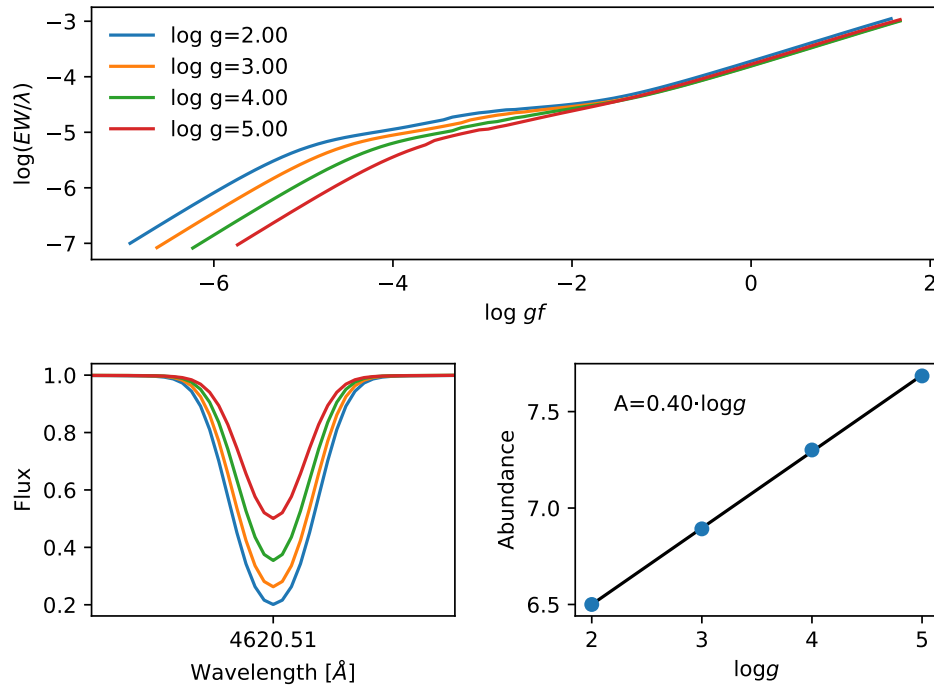


Figure 2.3: Upper panel: Curve of growth for same Fe II used in Figure 2.2 on the preceding page for four different $\log g$ values. Here it is the weak lines mostly affected by the change in $\log g$. Lower left panel: Synthetic spectra of the same line. The colour scale is the same. Lower right: The abundance for the line at different $\log g$. A strong correlation (0.40) is seen.

2.2.1.3 Abundance dependence

The abundance of a given element obviously has an effect on the EW. The more abundant an element is, the more photons can be absorbed thus increasing the EW. However, the relationship is not strictly linear. For weak lines (GIVE RANGE) EW is approximately linear with the abundance, however it reach a plateau where the core of the line saturates. In this regime the EW only increases slowly, until the absorption "spills" into the wings and the increase is again linear. However, for these strong lines the shape is no longer Gaussian. The curve of growth for the same Fe I line used in Figure 2.2 on the previous page is shown in Figure 2.4 on the facing page. Instead of EW it is common to use the reduced EW, $\log(EW/\lambda)^1$, which we will use more later. Instead of the abundance of a line, the oscillator strength, $\log gf$, is used.

¹ The reduced EW is useful since it normalizes Doppler-dependent phenomena, such as microturbulence and thermal broadening.

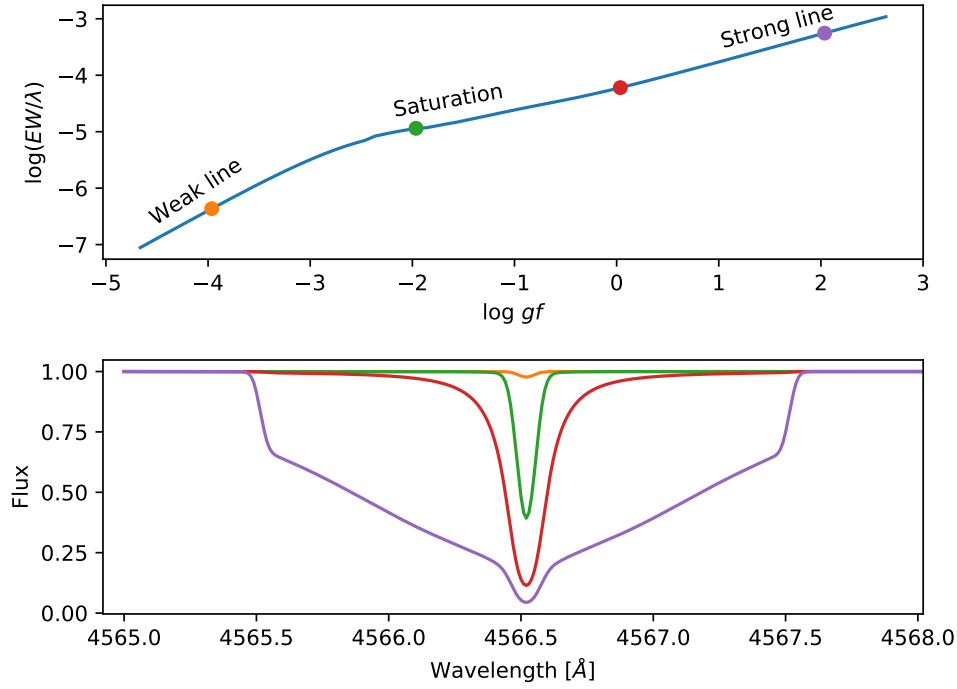


Figure 2.4: Upper panel: Curve of growth of the same Fe I line as used in Figure 2.2 on page 9. Four points are marked which is shown in the lower panel as a synthetic spectral line. The RW (proxy for EW) is clearly increasing with $\log gf$ (proxy for abundance).

2.2.1.4 Microturbulence

Small-scale motion, that is motion of material at length scales small compared to the unit optical depth, are called microturbulence, ζ_{micro} . This is not to be confused with macroturbulence, which is motion of material at scales larger than the unit optical depth. The latter is associated with granulation and will not be discussed further in this thesis. ζ_{micro} comes into play when looking at the curve of growth for saturated lines (i.e. between green and red points in Figure 2.4). If no ζ_{micro} is assumed, then the measured abundance is higher than predicted by models based on thermal and damping broadening alone. In Figure 2.5 on the following page is shown three curves of growth with $\zeta_{\text{micro}} = 0.5 \text{ km/s}, 2.5 \text{ km/s}, 5.0 \text{ km/s}$. As ζ_{micro} increases, so does the EW and hence the abundance.

The broadening of an absorption line measured by the shift in wavelength, $\Delta\lambda$, when ζ_{micro} is included is defined as:

$$\Delta\lambda = \frac{\lambda_0}{c} \sqrt{\frac{2kT}{m} + \zeta_{\text{micro}}^2} \quad (2.8)$$

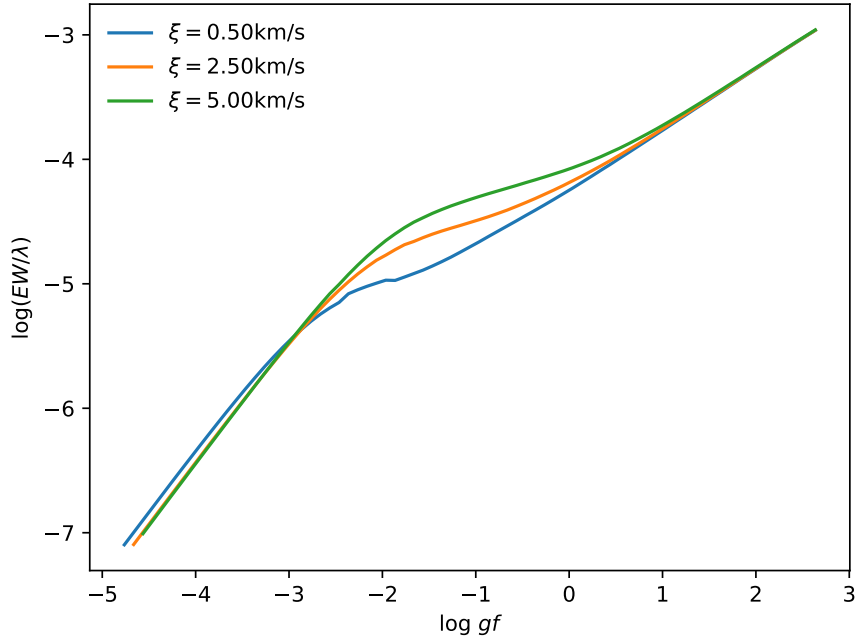


Figure 2.5: Curve of growth for three different values of ξ_{micro} . The EW is increasing with increasing ξ_{micro} .

where c is the speed of light, λ_0 is the rest wavelength of the given line, k is Boltzmann's constant, T is the temperature, and m is the mass of the atom. Setting $\xi_{\text{micro}} = 0 \text{ km/s}$, we end up with thermal broadening.

2.2.2 Stellar parameters for FGK stars

2.2.2.1 Line list and atomic data

2.2.2.2 Measuring EW

2.2.2.3 Determining abundances with MOOG

BIBLIOGRAPHY

- Aerts, C., Christensen-Dalsgaard, J., and Kurtz, D. W.: 2010, *Asteroseismology*
- Ammler-von Eiff, M., Santos, N. C., Sousa, S. G., Fernandes, J., Guillot, T., Israelian, G., Mayor, M., and Melo, C.: 2009, *A&A* 507, 523
- Andreasen, D. T., Sousa, S. G., Delgado Mena, E., Santos, N. C., Tsantaki, M., Rojas-Ayala, B., and Neves, V.: 2016, *A&A* 585, A143
- Andreasen, D. T., Sousa, S. G., Tsantaki, M., Teixeira, G. D. C., Mortier, A., Santos, N. C., Suárez-Andrés, L., Delgado Mena, E., and Ferreira, A. C. S.: 2017, *A&A* 585, A143
- Artigau, É., Kouach, D., Donati, J.-F., Doyon, R., Delfosse, X., Baratchart, S., Lacombe, M., Moutou, C., Rabou, P., Parès, L. P., Micheau, Y., Thibault, S., Reshetov, V. A., Dubois, B., Hernandez, O., Vallée, P., Wang, S.-Y., Dolon, F., Pepe, F. A., Bouchy, F., Striebig, N., Hénault, F., Loop, D., Saddlemyer, L., Barrick, G., Vermeulen, T., Dupieux, M., Hébrard, G., Boisse, I., Martioli, E., Alencar, S. H. P., do Nascimento, J.-D., and Figueira, P.: 2014, in *Society of Photo-Optical Instrumentation Engineers (SPIE) Conference Series*, Vol. 9147 of *Society of Photo-Optical Instrumentation Engineers (SPIE) Conference Series*, p. 15
- Baraffe, I., Homeier, D., Allard, F., and Chabrier, G.: 2015, *A&A* 577, A42
- Bensby, T., Feltzing, S., and Oey, M. S.: 2014, *A&A* 562, A71
- Blackwell, D. E. and Shallis, M. J.: 1977, *MNRAS* 180, 177
- Boyajian, T. S., von Braun, K., van Belle, G., McAlister, H. A., ten Brummelaar, T. A., Kane, S. R., Muirhead, P. S., Jones, J., White, R., Schaefer, G., Ciardi, D., Henry, T., López-Morales, M., Ridgway, S., Gies, D., Jao, W.-C., Rojas-Ayala, B., Parks, J. R., Sturmann, L., Sturmann, J., Turner, N. H., Farrington, C., Goldfinger, P. J., and Berger, D. H.: 2012, *ApJ* 757, 112
- Casagrande, L., Ramírez, I., Meléndez, J., Bessell, M., and Asplund, M.: 2010, *A&A* 512, A54

- Conod, U., Blind, N., Wildi, F., and Pepe, F.: 2016, in *Society of Photo-Optical Instrumentation Engineers (SPIE) Conference Series*, Vol. 9909 of *Proceedings of the SPIE*, p. 990941
- Delfosse, X., Donati, J.-F., Kouach, D., Hébrard, G., Doyon, R., Artigau, E., Bouchy, F., Boisse, I., Brun, A. S., Hennebelle, P., Widemann, T., Bouvier, J., Bonfils, X., Morin, J., Moutou, C., Pepe, F., Udry, S., do Nascimento, J.-D., Alencar, S. H. P., Castilho, B. V., Martioli, E., Wang, S. Y., Figueira, P., and Santos, N. C.: 2013, in L. Cambresy, F. Martins, E. Nuss, and A. Palacios (eds.), *SF2A-2013: Proceedings of the Annual meeting of the French Society of Astronomy and Astrophysics*, pp 497–508
- Dotter, A., Chaboyer, B., Jevremović, D., Kostov, V., Baron, E., and Ferguson, J. W.: 2008, *ApJS* 178, 89
- Follert, R., Dorn, R. J., Oliva, E., Lizon, J. L., Hatzes, A., Piskunov, N., Reiners, A., Seemann, U., Stempels, E., Heiter, U., Marquart, T., Lockhart, M., Anglada-Escude, G., Löwinger, T., Baade, D., Grunhut, J., Bristow, P., Klein, B., Jung, Y., Ives, D. J., Kerber, F., Pozna, E., Paufigue, J., Kaeufl, H. U., Origlia, L., Valenti, E., Gojak, D., Hilker, M., Pasquini, L., Smette, A., and Smoker, J.: 2014, in *Society of Photo-Optical Instrumentation Engineers (SPIE) Conference Series*, Vol. 9147 of *Society of Photo-Optical Instrumentation Engineers (SPIE) Conference Series*, p. 19
- Girardi, L., Bressan, A., Bertelli, G., and Chiosi, C.: 2000, *A&A Supp.* 141, 371
- Gray, D. F.: 2005, *The Observation and Analysis of Stellar Photospheres*, 3rd ed.
- Kippenhahn, R. and Weigert, A.: 1994, *Stellar Structure and Evolution*, Springer-Verlag
- Kjeldsen, H. and Bedding, T. R.: 1995, *A&A* 293, 87
- Kotani, T., Tamura, M., Suto, H., Nishikawa, J., Sato, B., Aoki, W., Usuda, T., Kurokawa, T., Kashiwagi, K., Nishiyama, S., Ikeda, Y., Hall, D. B., Hodapp, K. W., Hashimoto, J., Morino, J.-I., Okuyama, Y., Tanaka, Y., Suzuki, S., Inoue, S., Kwon, J., Suenaga, T., Oh, D., Baba, H., Narita, N., Kokubo, E., Hayano, Y., Izumiura, H., Kambe, E., Kudo, T., Kusakabe, N., Ikoma, M., Hori, Y., Omiya, M., Genda, H., Fukui, A., Fujii, Y., Guyon, O., Harakawa, H., Hayashi, M., Hidai, M., Hirano, T., Kuzuhara, M., Machida, M., Matsuo, T., Nagata, T., Onuki, H., Ogihara, M., Takami, H., Takato, N., Takahashi, Y. H., Tachinami, C., Terada, H., Kawahara, H., and Yamamuro, T.: 2014, in *Society of Photo-Optical Instrumentation Engineers (SPIE) Conference Series*, Vol. 9147 of *Society of Photo-Optical Instrumentation Engineers (SPIE) Conference Series*, p. 14

- Lebzelter, T., Heiter, U., Abia, C., Eriksson, K., Ireland, M., Neilson, H., Nowotny, W., Maldonado, J., Merle, T., Peterson, R., Plez, B., Short, C. I., Wahlgren, G. M., Worley, C., Aringer, B., Bladh, S., de Laverny, P., Goswami, A., Mora, A., Norris, R. P., Recio-Blanco, A., Scholz, M., Thévenin, F., Tsuji, T., Kordopatis, G., Montesinos, B., and Wing, R. F.: 2012, *A&A* **547**, A108
- Lindgren, S., Heiter, U., and Seifahrt, A.: 2016, *A&A* **586**, A100
- Meléndez, J. and Barbuy, B.: 1999, *ApJS* **124**, 527
- Mucciarelli, A., Pancino, E., Lovisi, L., Ferraro, F. R., and Lapenna, E.: 2013, *ApJ* **766**, 78
- Önehag, A., Heiter, U., Gustafsson, B., Piskunov, N., Plez, B., and Reiners, A.: 2012, *A&A* **542**, A33
- Origlia, L., Oliva, E., Baffa, C., Falcini, G., Giani, E., Massi, F., Montegriffo, P., Sanna, N., Scuderi, S., Sozzi, M., Tozzi, A., Carleo, I., Gratton, R., Ghinassi, F., and Lodi, M.: 2014, in *Society of Photo-Optical Instrumentation Engineers (SPIE) Conference Series*, Vol. 9147 of *Society of Photo-Optical Instrumentation Engineers (SPIE) Conference Series*, p. 1
- Quirrenbach, A., Amado, P. J., Caballero, J. A., Mundt, R., Reiners, A., Ribas, I., Seifert, W., Abril, M., Aceituno, J., Alonso-Floriano, F. J., Ammler-von Eiff, M., Antona Jiménez, R., Anwand-Heerwart, H., Azzaro, M., Bauer, F., Barrado, D., Becerril, S., Béjar, V. J. S., Benítez, D., Berdiñas, Z. M., Cárdenas, M. C., Casal, E., Claret, A., Colomé, J., Cortés-Contreras, M., Czesla, S., Doellinger, M., Dreizler, S., Feiz, C., Fernández, M., Galadí, D., Gálvez-Ortiz, M. C., García-Piquer, A., García-Vargas, M. L., Garrido, R., Gesa, L., Gómez Galera, V., González Álvarez, E., González Hernández, J. I., Grözinger, U., Guàrdia, J., Guenther, E. W., de Guindos, E., Gutiérrez-Soto, J., Hagen, H.-J., Hatzes, A. P., Hauschildt, P. H., Helmling, J., Henning, T., Hermann, D., Hernández Castaño, L., Herrero, E., Hidalgo, D., Holgado, G., Huber, A., Huber, K. F., Jeffers, S., Joergens, V., de Juan, E., Kehr, M., Klein, R., Kürster, M., Lamert, A., Lalitha, S., Laun, W., Lemke, U., Lenzen, R., López del Fresno, M., López Martí, B., López-Santiago, J., Mall, U., Mandel, H., Martín, E. L., Martín-Ruiz, S., Martínez-Rodríguez, H., Marvin, C. J., Mathar, R. J., Mirabet, E., Montes, D., Morales Muñoz, R., Moya, A., Naranjo, V., Ofir, A., Oreiro, R., Pallé, E., Panduro, J., Passegger, V.-M., Pérez-Calpena, A., Pérez Medialdea, D., Perger, M., Pluto, M., Ramón, A., Reboló, R., Redondo, P., Reffert, S., Reinhardt, S., Rhode, P., Rix, H.-W., Rodler, F., Rodríguez, E., Rodríguez-López, C., Rodríguez-Pérez, E., Rohloff, R.-R., Rosich, A., Sánchez-Blanco, E., Sánchez Carrasco, M. A., Sanz-Forcada, J., Sarmiento, L. F., Schäfer, S., Schiller, J., Schmidt, C., Schmitt, J. H. M. M., Solano, E., Stahl, O., Storz, C., Stürmer, J., Suárez, J. C., Ulbrich, R. G.,

- Veredas, G., Wagner, K., Winkler, J., Zapatero Osorio, M. R., Zechmeister, M., Abellán de Paco, F. J., Anglada-Escudé, G., del Burgo, C., Klutsch, A., Lizon, J. L., López-Morales, M., Morales, J. C., Perryman, M. A. C., Tulloch, S. M., and Xu, W.: 2014, in *Society of Photo-Optical Instrumentation Engineers (SPIE) Conference Series*, Vol. 9147 of *Society of Photo-Optical Instrumentation Engineers (SPIE) Conference Series*, p. 1
- Ramírez, I. and Meléndez, J.: 2005, *ApJ* **626**, 446
- Rayner, J., Bond, T., Bonnet, M., Jaffe, D., Muller, G., and Tokunaga, A.: 2012, in *Ground-based and Airborne Instrumentation for Astronomy IV*, Vol. 8446 of *Proceedings of the SPIE*, p. 84462C
- Rayner, J., Tokunaga, A., Jaffe, D., Bonnet, M., Ching, G., Connelley, M., Kokubun, D., Lockhart, C., and Warmbier, E.: 2016, in *Society of Photo-Optical Instrumentation Engineers (SPIE) Conference Series*, Vol. 9908 of *Proceedings of the SPIE*, p. 990884
- Recio-Blanco, A., Bijaoui, A., and de Laverny, P.: 2006, *MNRAS* **370**, 141
- Santos, N. C., Sousa, S. G., Mortier, A., Neves, V., Adibekyan, V., Tsantaki, M., Delgado Mena, E., Bonfils, X., Israelian, G., Mayor, M., and Udry, S.: 2013, *A&A* **556**, A150
- Sousa, S. G., Santos, N. C., Mayor, M., Udry, S., Casagrande, L., Israelian, G., Pepe, F., Queloz, D., and Monteiro, M. J. P. F. G.: 2008, *A&A* **487**, 373
- Torres, G., Andersen, J., and Giménez, A.: 2010, *Astronomy and Astrophysics Reviews* **18**, 67
- Torres, G., Fischer, D. A., Sozzetti, A., Buchhave, L. A., Winn, J. N., Holman, M. J., and Carter, J. A.: 2012, *ApJ* **757**, 161
- Torres, G., Winn, J. N., and Holman, M. J.: 2008, *ApJ* **677**, 1324
- Tsantaki, M., Sousa, S. G., Adibekyan, V. Z., Santos, N. C., Mortier, A., and Israelian, G.: 2013, *A&A* **555**, A150
- Tsantaki, M., Sousa, S. G., Santos, N. C., Montalto, M., Delgado-Mena, E., Mortier, A., Adibekyan, V., and Israelian, G.: 2014, *A&A* **570**, A80
- Valenti, J. A. and Fischer, D. A.: 2005, *ApJS* **159**, 141